The concept of differential hardness in depth sensing indentation

2003 New J. Phys. 5 15

(http://iopscience.iop.org/1367-2630/5/1/315)

New Journal of Physics
An Institute of Physics and Deutsche Physikalische Gesellschaft Journal

The concept of differential hardness in depth sensing indentation

B Wolf and A Richter
University of Applied Sciences Wildau, Surface Technology Laboratories, Bahnhofstraße 1, D-15745 Wildau, Germany
E-mail: bwolf@igw.tfh-wildau.de

New Journal of Physics **5** (2003) 15.1–15.17 (http://www.njp.org/)
Received 25 November 2002, in final form 24 January 2003
Published 3 March 2003

Abstract. Since in-depth sensing indentation load–depth data of the entire loading–unloading cycle are available, more information than a single hardness value and an elastic modulus can be extracted from the experimental data. The conventional hardness $H(h) = F(h)/A_C(h)$ and the differential hardness $H_d(h) = \mathrm{d}F/\mathrm{d}A_C$ are calculated as continuous functions of depth h and compared to each other in this paper (F: load, A_C: contact area). It turns out that H_d describes the momentary material resistance to deformation, whereas H integrates over deformation states from first tip–sample contact to current penetration h. This difference is particularly important for materials not homogeneous in depth (e.g. layer systems), and for situations where time-dependent external factors influence the momentary deformation resistance. Photoplasticity is considered as an example for the latter.

Contents

PII: S1367-2630(03)56588-0

1. Introduction

In traditional microhardness testing, the area of the imprint A is measured after complete unloading using some surface visualization technique, commonly light microscopy. In addition, scanning electron microscopy and scanning force microscopy have been used recently [1]–[3]. The hardness H as a measure of material resistance to irreversible deformation is then calculated as $H = F/A$. The successful development of scanning probe microscopy, STM and atomic force microscopy (AFM), between 1980 and 1990 gave rise to improvements in depth sensing indentation [4]–[6], resulting in commercial instruments such as the Nanoindenter [7] or the HYSITRON transducer [8]. In these instruments, load F and depth h are recorded simultaneously, and from the obtained $F(h)$-function hardness and elastic modulus are derived. The so-called Oliver–Pharr approach [9], a further development of ideas of Doerner and Nix [10], became the standard technique of data analysis. After onset of plastic deformation (yielding), the loading curve is an overlap of both plastic and elastic deformation, and the relative percentages of these contributions to the depth are *a priori* not known. In contrast to this, the unloading curve is commonly regarded as purely elastic, apart from situations with strong viscosity, as found with polymers, or in the case of phase transformations that occur in Si, e.g. [11]. For the reason of simple separation of plasticity and elasticity the unloading curve is used as the main source of information in data analysis based on the Oliver–Pharr approach. The loading curve—though containing a lot of, however, not easily accessible information—is commonly not used for indentation experiment analysis.

In this paper we aim to assign each point of the loading curve a corresponding hardness value. This requires knowledge of the contact depth h_C as a function of the total penetration depth h. This function can be obtained by performing a multicycling indent, i.e. a sequence of n reloading/unloading cycles with increasing maximum load from cycle to cycle. The multicycling delivers a set of n data pairs (h_C, h) where each data pair (h_C, h) is inferred from one unloading process. The discrete data pairs $(h_C, h)_i$, $i = 1, \ldots, n$, can be used to establish a fit-function $h_C(h)$. Using this function the conventional hardness is calculated according to $H(h) = F(h)/A_C(h_C(h)) = F(h)/A_C(h)$. A_C is the contact area: the cross-sectional area of the indenter when cut at a distance h_C from its end. Normally A_C is determined as a function of h_C in a calibration procedure [9], but replacing h_C by the fit-function $h_C(h)$ delivers $A_C(h)$. We called this deduction of a continuous hardness function $H(h)$ from multicycling indentation the '$h_C(h)$ technique'. A brief description of the $h_C(h)$ technique is given in sections 3 and 4.1. A more detailed discussion of the $h_C(h)$ technique can be found in [12].

Apart from conventional hardness $H = F/A_C$ a differential entity $H_d = \mathrm{d}F/\mathrm{d}A_C$ can be considered. This 'differential hardness' is obviously more sensitive to the momentary material resistance to indenter penetration than $H(h)$, which involves the entire material response from the first indenter–sample contact to penetration h. It is shown in section 4.3 that the difference between H and H_d is proportional to $(\mathrm{d}H/\mathrm{d}h)$. A separate consideration of both H and H_d is therefore useful if the hardness is depth dependent. This is obviously the case for samples which are inhomogeneous in depth (layer systems). However, homogeneous materials can also exhibit hardness which depends on depth and consequently on indentation size. The material displacement during indentation takes advantage of defects, as dislocations in ductile crystals, micro- and nanocracks in very brittle matter (quasicrystals, for instance [13]), grain boundaries, or free volumes (e.g. holes and pores in glass). With respect to homogeneous materials we can differentiate between two situations.

(i) The material contains a large number of defects. In this case, the deformation is based on defects which already exist in the material. We obtain a hardness which is almost constant provided that the indenter obeys self-similarity (as for pyramids or cones, but not in the case of spheres).

(ii) The material contains a very small number of defects. Then the deformation is mainly based on defects which are generated during indentation. Thus, the material does not remain homogeneous after the beginning of indentation, and the hardness depends on the indentation history. The contact pressure can rise to values close to the theoretical limit of strength in very perfect single crystals, and then significantly drop after the sudden formation of first dislocations (visible as yield steps, so-called 'pop-in'-phenomena, in the load–depth curve $F(h)$ [14]–[16]). Once dislocations have been formed, they can easily multiply and facilitate further deformation. However, dislocation mobility will decrease with increasing dislocation density. Similar considerations can be made with respect to cracks. A detailed discussion of the indentation size effect in bulk materials, thin films and nanolayer composites can be found in [17]–[19].

Finally, the concept of differential hardness proves useful for samples, the momentary hardness of which can be controlled by external factors, e.g. by illumination (photoplasticity) [20]–[22].

Since the calculation of both $H(h)$ and $H_d(h)$ requires knowledge of the $h_C(h)$-function, which in turn is derived from multicycling, this paper addresses the following considerations:

- multicycling and determination of $h_C(h)$,
- theoretical determination of $H(h)$,
- theoretical determination of $H_d(h)$,
- application of these concepts to selected samples.

2. Experimental details

All experiments were performed using a HYSITRON Triboscope attached to either a Nanoscope E scanning force microscope of Digital Instruments (now VEECO) at TFH Wildau, or to a Nanoscope III Dimension 3000 SFM system at TU Dresden (the latter being used for photoplastic experiments only; see section 5 for a detailed discussion of this subject). The main device of the Triboscope is an electrostatic transducer: a three-plate capacitor, the mid-plate of which carries the indentation diamond mounted to a stylus. Application of a DC voltage up to 600 V results in an electrostatic force (maximum load depending on capacitor plate spacing and area, maximum 6.3 mN in our configuration) that drives the diamond tip into the specimen. The change of the capacitance is simultaneously recorded as a measure of penetration depth. The primary data (voltage U, capacitance change ΔC) are converted into (load F, depth h), resulting in a $F(h)$ curve. After complete unloading the impression site can be scanned with the same tip. A more detailed description of the indenter is given in [23].

We tested samples from three different materials: copper, diamond-like carbon (DLC) coatings on silicon, and ZnSe. Details of sample characteristics are given below.

(i) Single-crystalline copper grown by the Bridgman technique at Universität Saarbrücken, Werkstoffwissenschaften, Lehrstuhl Professor Vehoff. The crystal was oriented by the x-ray Laue technique, cut into slices, ground and polished down to a finish of 0.25 μm using

standard metallographic procedures, and finally electrochemically polished (60% H_3PO_4 solution, platinum electrode, 1.9 V DC at 20 °C for 30 s). This sample was used as a representative of materials which are inherently homogeneous in depth, but show a distinct indentation size effect owing to indentation-induced defects (dislocations).

(ii) (100)-oriented silicon wafers, coated by DLC. The DLC coating was performed using high-current arc deposition (HCA technique) at Fraunhofer Institute IWS Dresden. The DLC layers are amorphous. Two samples are considered here.

- Sample 1, coated with 960 nm DLC, as a representative of samples with extended elastic contact, and where the layer is thick enough to obtain a hardness plateau (negligible substrate impact).
- Sample 2, coated with 113 nm DLC. This sample exhibits both an extended region of elastic contact, and at deeper penetrations a strong hardness drop due to the growing influence of the substrate. It is thus a representative of samples with particularly strong hardness gradients.

(iii) Photoplastic experiments were conducted on a single-crystalline ZnSe sample purchased from Crystec GmbH, Berlin [24]. ZnSe is a II–VI-semiconductor the band-gap of which (2.6 eV) allows the inducing of reversible hardness changes by visible light.

3. Multicycling testing

Multicycling testing refers to performing a sequence of n loading–unloading cycles in one experiment at the same lateral position. It enables us to obtain hardness and elastic modulus as depth-dependent data. Besides saving time, the data collection does not suffer from lateral inhomogeneities of the sample. We should note that such a multicycling test takes much more time than a single indent, hence drift correction is an important issue. In figure 1 (left) the load–time regime of a multi-indent, comprising 18 cycles, is shown, whereas in the right part of figure 1 the resulting load–depth curve after application to single-crystalline copper (100) is depicted. This experiment delivers 18 data sets $(F_t, h_t, h_C, A_C, \ldots)_i$, $i = 1, \ldots, 18$. The symbols stand for: F_t, maximum load of a loading/unloading cycle; h_t, maximum penetration depth when applying F_t; h_C, contact depth when applying F_t; A_C, contact area related to F_t. The hardness

$$H_i = (F_t/A_C)_i \tag{1}$$

can be either assigned to h_t or to h_C, i.e. we obtain $H(h_t)_i$ or $H(h_C)_i$, respectively.

It is now possible to consider a quantity

$$H_{di} = (\Delta F_t/\Delta A_C)_i = [(F_{ti+1} - F_{ti})/(A_{Ci+1} - A_{Ci})] \tag{2}$$

that we will call differential hardness. In figure 2, H_i and H_{di}, derived from the multi-indent into copper (figure 1), have been plotted against the total penetration depth h_t. (When we consider F_t and h_t as continuously changing values during a loading cycle we can write F instead of F_{ti}, and h instead of h_{ti}, i.e. h is the total depth which is related to application of load F.) Two observations are obvious from figure 2:

(i) the hardness decreases with increasing load (normal indentation size effect ISE), and

(ii) $H_d < H$.

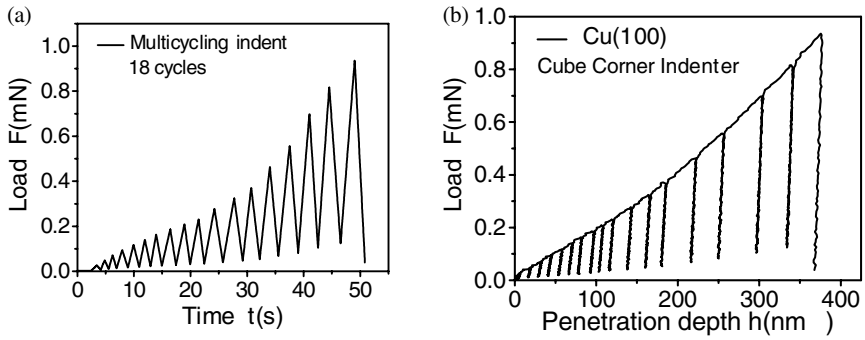

Figure 1. Load–time scheme of a multicycling nanoindentation (left) and resulting load–depth curve $F(h)$ for application to a copper single crystal.

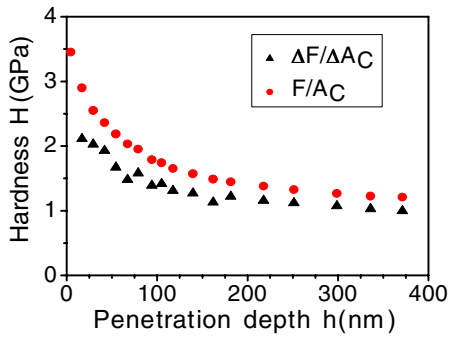

Figure 2. Conventional hardness F/A_C and differential hardness $\Delta F/\Delta A_C$ derived from the multi-indent shown in figure 1 (copper (100)).

The ISE of copper can be explained using the model of geometrically necessary dislocations [22, 23]. A smaller indent generates on average a higher dislocation density than a larger one, and owing to dislocation–dislocation interaction the hardness increases with the root of the dislocation density, i.e. with smaller penetrations.

The relation $H > H_d$ will be considered in more detail in section 4.3. It can, however, be qualitatively understood following this argument: $H(h)$ is an entity averaging over all deformation states from depth $= 0$ to h. In contrast to this, H_d describes the momentary sample response to deformation. When H and H_d are decreasing with h, H must be larger than H_d, since H averages over situations where the deformation resistance was larger and larger in comparison to the present situation.

For theoretical calculations the knowledge of the relation between contact depth h_C and total depth $h_t = h$ is interesting, since this relation is the key to separate the total penetration into an elastic and a plastic part. This relation has been studied in detail in [12]. Experimentally the $h_C(h)$ relation can be obtained from a multicycling experiment that delivers n pairs (h_C, h_t) which can be fitted to a fit-function $h_C(h)$. This function for copper, inferred from the multicycling test of figure 1, is shown in figure 3. Because of the high ductility of copper h_C is only a small fraction (2%) smaller than h in case of larger depths where the plastic zone is fully developed. This is different for less ductile materials like glass, ceramics or semiconductors, where h_C is much smaller than h. For examples of this class of materials consider figures 6(b) and 7(b).

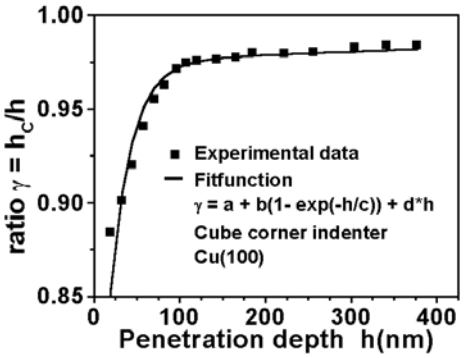

Figure 3. Ratio $\gamma = h_C/h$ between contact depth and total penetration depth extracted from the multi-indent of figure 1. The parameters of the fit-function are $a = 0.703$, $b = 0.272$, $c = 24.3$ nm, $d = 1.9 \times 10^{-5}$ nm^{-1}.

4. Determination of hardness $H(h)$ and differential hardness $H_d(h)$ from the load–depth curve $F(h)$

4.1. Determination of $H(h)$ using the $h_C(h)$ approach

In nanoindentation experiments the indenter can never be regarded as of ideal geometric shape. As a consequence the indenter cross-sectional area must be determined in a calibration procedure. This calibration must be repeated after suitable periods (depending on how intensely the indenter is used, typically once a month), since the indenter tip is subject to progressive blunting, particularly when testing hard materials. The standard technique of tip calibration is to perform a series of indents into a calibration standard with different loads and consequently penetration depths. The calibration standard should be a homogeneous and isotropic material, which is not affected by reactions in air. A recommended material is fused silica, which is used in our laboratory, too. A series of n indents of different loads F_i delivers n values of contact depth $h_{Ci}(F_i)$, $i = 1, \ldots, n$. Instead of individual single indentations, a multi-indent can also be used for tip area calibrations.

The corresponding contact areas $A_{Ci}(h_{Ci})$ are determined such that the analysis of the elastic unloading curves delivers the correct value of the elastic modulus E ($E = 70$ GPa for fused silica), which has been measured by an independent technique (measurement of the speed of ultrasonic waves). Now, the n pairs (h_{Ci}, A_{Ci}) can be fitted to a continuous function $A_C(h_C)$, which is a universal function, valid for all materials. One can use any mathematical function that fits the data pairs; the preferred expression is $A_C = C_2 h_C^2 + C_1 h_C + C_{1/2} h_C^{1/2}$ (C_i: fit parameter). The parabolic term describes the behaviour of an ideal pyramid, the linear term that of a parabola of rotation (or a sphere, when restricting to small depths compared to the radius), and the root is related to tip truncation. The described calibration procedure was suggested in [9]. Another possibility of indenter calibration is the three-dimensional reconstruction of the indenter shape from AFM imaging, which we have described in [27]. We found, however, that $A_C(h_C)$ can be up to 30% larger in the last case owing to tip dirtification. Soft contamination layers increase the apparent volume of the indenter as determined by AFM mapping, but are not 'active' volume (i.e. are easily displaced) when indenting hard samples.

Different materials have different relations between total depth h and contact depth h_C

owing to different percentages of the elastic contribution to the total depth h. If the contact depth h_C is substituted by a mathematical expression of h and inserted into $A_C(h_C)$ one obtains $A_C(h_C(h)) = A_C(h)$. In contrast to $A_C(h_C)$ as a universal function the expression $A_C(h)$ is a very special one, valid for the material under investigation only.

Having determined $A_C(h)$, the hardness can be calculated according to

$$H(h) = F(h)/A_C(h). \tag{3}$$

We found that for the measured sample of copper the function $h_C(h)$ can be fitted by an expression

$$h_C(h) = [a + b(1 - \exp(-h/c)]h + dh^2 \tag{4}$$

with fit parameters a, b, c and d, their numerical values are given in the legend of figure 3. The formalism can be now applied to any $F(h)$ curve of copper to assign each depth a corresponding hardness value. In figure 4 a load–depth curve of a single indent into Cu(100) is shown on the left, and the right plot depicts the resulting hardness–depth function as derived from application of the $h_C(h)$ formalism to the left curve.

It is often claimed that load–depth curves obtained with pyramid indenters were parabolic curves, i.e. exhibit a $F \sim h^2$ behaviour. Figure 4 clearly demonstrates that this statement is wrong. In fact the $F(h)$ curve is nearly linear. For better recognition a 'theoretical' $F \sim h^2$ curve was inserted into figure 4. This almost linear behaviour is not due to indenter truncation. The cube corner in use has a radius of curvature $R \approx 150$ nm, i.e. for depths >100 nm it can be regarded as almost ideal. The main reason for the nonparabolic $F(h)$ curve is the ISE. Due to the decreasing hardness the load rises less quickly than the contact area does with increasing depth. When using the model of geometrically necessary dislocations [25, 26] the hardness behaves: $H \sim h^{-1/2}$. For the load we find $F = HA_C \sim h^{-1/2}h^2 \sim h^{3/2}$ which can reasonably explain the results of figure 4.

One of the particular advantages of the $h_C(h)$ technique is that it delivers the hardness as a continuous function of depth, and provided that the load–depth curve $F(h)$ is smooth, at least in several segments, $H(h)$ is also a smooth function and suitable for differentiation, as is used in the following section.

4.2. Differential hardness $H_d(h)$

Instead of calculating the 'conventional' hardness as load divided by impression area, one can also consider the corresponding differential entity

$$H_d = \mathrm{d}F/\mathrm{d}AC. \tag{5}$$

This quantity describes the instantaneous material resistance to mechanical deformation, whereas the conventional hardness $H = F/A_C$ provides an average measure of the deformation resistance from the very beginning of tip penetration up to unloading. It is obvious that H_d has the following properties.

(i) $H_d = H$ in case of constant H, since for $H =$ constant we have $A_C \sim F$ and $\mathrm{d}F/\mathrm{d}A_C = F/A_C$.

(ii) In comparison to H the differential hardness H_d is more sensitive to the material properties directly beneath the indenter tip, and less sensitive to the material at the outermost surface.

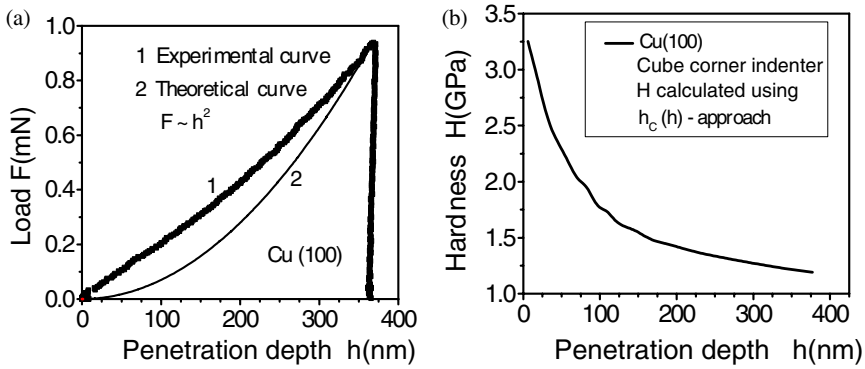

Figure 4. Load–depth curve of a cube-corner nanoindent (single indent) into Cu(100) on the left, and resulting conventional hardness $H(h) = F(h)/A_C(h)$ obtained by using the $h_C(h)$ formalism. A comparison with figure 2 shows the coincidence of the hardness data inferred by the multicycling and by the $h_C(h)$ approach, respectively.

For a layer–substrate system the substrate impact is stronger on H_d than on H. For a multilayer system, where the tip penetrated to layer n, a layer k, with $k < n$, has a smaller, and a layer l, with $l > n$, has a stronger impact on the currently measured H_d data. A more detailed comparison between H and H_d is made in section 4.3.

The easiest access to H_d provides a multi-indent with n loading/unloading segments with load increments from segment to segment. The calculation is done according to equation (2), and the result for copper is illustrated in figure 2. In the case of copper the mean contact pressure (hardness) decreases continuously, apart from the very first state of penetration which is purely elastic (not shown in the figure). In the following, the situation of a hard and stiff layer on a much softer and more compliant substrate is considered, namely a layer of DLC on silicon. Owing to both high hardness and large elastic modulus of DLC, there is an extended depth region of pure elastic contact where the contact pressure H increases according to $H \sim \sqrt{h}$. At a depth of 10–15% of the tip radius ($R_{tip} \approx 150$ nm) the DLC starts to yield. For single crystals the yielding becomes often visible by a pop-in, a sudden depth excursion due to nucleation and propagation of dislocations [14]–[16]. Such a pop-in will not occur in a nanocrystalline or amorphous DLC layer. After onset of plastic deformation the contact pressure (hardness) will further rise, which is due to the increase of the constraint factor C. The constraint factor C is the ratio between hardness and yield strength Y [1]:

$$C = H/Y. \tag{6}$$

We find $C \approx 1$ at initial yielding, and after formation of the full plastic zone, C attains a saturation value C_{sat}, depending on the nature of the material. For ductile matter (metals like steel) we have $C_{sat} \approx 3$, for brittle materials C_{sat} can be much larger, up to 40 [28]. The saturation of C, resulting in a constant hardness, is related to obtaining self-symmetry of the imprint, i.e. when using a pyramid indenter, the penetration must be larger than the spherical cap due to tip blunting. When the penetration exceeds 10% of the layer thickness, the substrate hardness will start to influence the measured hardness. Table 1 summarizes the stages of contact pressure evolution for a layer–substrate system (hard layer on a softer substrate).

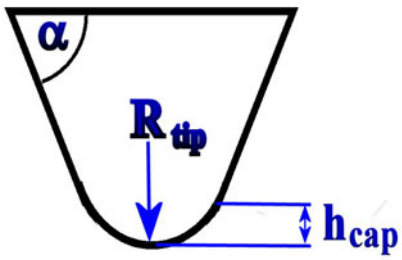

Figure 5. Schematic illustration of a blunted pointed indenter. A spherical cap is added to the trunk of a cone or pyramid. The transition from the cap to the cone or pyramid occurs without discontinuity for a height of the cap $h_{cap} = R_{tip}(1 - \cos\alpha)$.

Table 1. Overview on contact pressure development during nanoindentation.

Penetration depth h	Situation
$<(0.1, \ldots, 0.15)R_{tip}$	Pure elastic contact, $H \sim \sqrt{h}$
$>(0.1, \ldots, 0.15)R_{tip}$ $<2h_{cap}$	Development of the plastic zone, H slowly increases with the trend of saturation
$>2h_{cap}$ $<0.1d$	Hardness plateau
$>2h_{cap}$ $>0.1d$	No hardness plateau, substrate influence decreases hardness before maximum layer hardness is attained

Besides the tip radius R_{tip} the height of the spherical cap h_{cap} is a critical parameter for measurement of true layer properties. When 10% of the layer thickness d is smaller than $2h_{cap}$ one will never measure the 'true' layer hardness. Figure 5 reveals that

$$h_{cap} = R_{tip}(1 - \cos\alpha) \tag{7}$$

where α is the angle between the horizontal direction and the side plane of the pyramid. For a cube-corner indenter one obtains $h_{cap} = 0.3R_{tip}$.

In figure 6 nanoindentation results for 960 nm DLC on silicon are summarized. In this case the layer is thick enough to allow the hardness to achieve a plateau. On the other hand, the penetration depth is small enough to avoid a significant substrate influence, even for the highest load of the indentation machine (6 mN). Figure 6(a) depicts the load–depth curve for 5 mN load, and in figure 6(c) conventional hardness H and differential hardness H_d from a series of multicycling indents are shown. Since ΔF and ΔA_C are much smaller than F and A_C the data scattering of H_d is larger than that of H. In figure 6(d) curves of $H(h)$ and $H_d(h)$ are shown that were continuously derived from the $F(h)$ curve of figure 6(a). H was determined using the $h_C(h)$ technique. The necessary value of $\gamma = h_C/h$ was derived from those multi-indents, the results of which are shown in figure 6(c). The curve $H_d(h)$ was calculated in the following way:

$$H_d = \mathrm{d}F/\mathrm{d}A_C = (\mathrm{d}F/\mathrm{d}h)(\mathrm{d}h/\mathrm{d}A_C) = (\mathrm{d}F/\mathrm{d}h)(\mathrm{d}A_C/\mathrm{d}h_C)^{-1}(\mathrm{d}h_C/\mathrm{d}h)^{-1}. \tag{8}$$

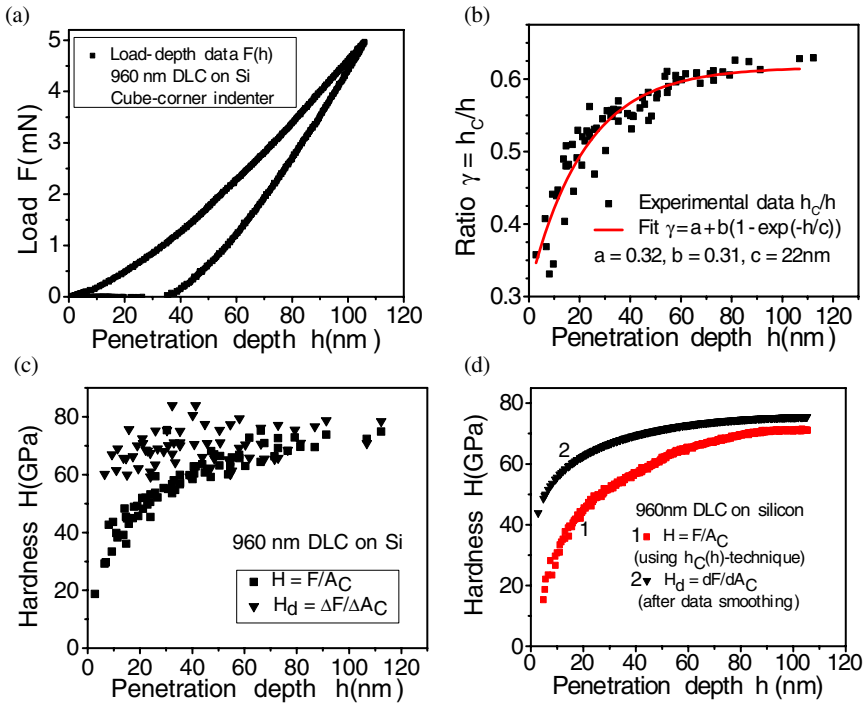

Figure 6. (a) Load–depth curve of a cube-corner nanoindent into 960 nm DLC on Si, (b) corresponding ratio of contact depth over total depth, (c) conventional hardness H and differential hardness H_d derived from multicycling tests and (d) from a single indent using the $h_C(h)$ technique.

To determine the necessary differential quotients $F(h)$, $A_C(h_C)$ and $h_C(h)$ were fitted to analytical functions after appropriate data smoothing, and the resulting functions were analytically differentiated. The results (figure 6(d)) coincide with the numerically determined values (figure 6(c)) but with considerably smaller noise.

The same procedure was applied to a sample of 113 nm DLC on silicon; the corresponding results are shown in figures 7(a)–(d). In this case the layer is too small to measure the 'true' layer hardness. 10% of the thickness is 11 nm which is smaller than $(10, \ldots, 15\%)$ of R_{tip} $(15, \ldots, 23$ nm), and smaller than the height of the spherical cap (45 nm). From measurements of the elastic modulus E by surface acoustic waves a similar modulus as in the case of the 960 nm thick layer was derived (960 nm thick DLC: $E = (540 \pm 30)$ GPa, 113 nm DLC: $E = (570 \pm 40)$ GPa), hence the 'true' layer hardness may be similar to that of the thicker layer, around 70 GPa, too.

When comparing H and H_d the following facts can be noted (see figures 7(c) and (d)):

(i) in the range of elastic contact ($h = 0, \ldots, \approx 20$ nm) H_d rises more quickly than H, and $H_d > H$ ($H_d \approx 1.5\ H$),

(ii) H_d attains its maximum at a smaller depth than H,

(iii) $H \approx H_d$ at the maximum H,

(iv) $H_d < H$ for depths larger than 70 nm, i.e. where $\mathrm{d}H/\mathrm{d}h < 0$,

(v) $H_d \to H$ when H becomes constant.

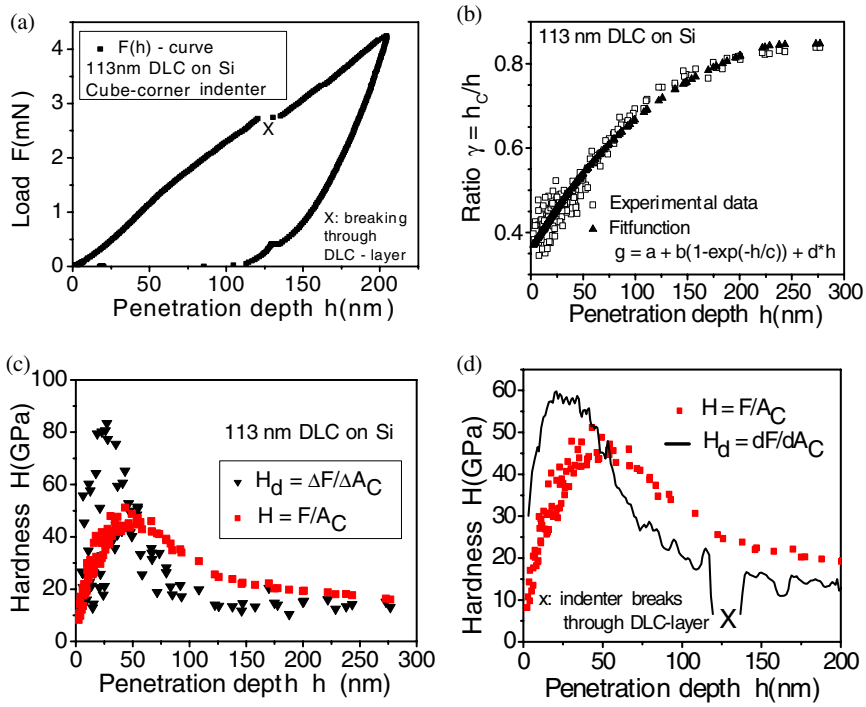

Figure 7. (a) Load–depth curve of a cube-corner nanoindent into 113 nm DLC on Si, (b) corresponding ratio of contact depth over total depth and (c) conventional hardness H and differential hardness H_d derived from multicycling tests. In (d) H derived from multicycling is compared to H_d derived from a single indent using numerical differentiation instead of analytical approximation and analytical differentiation. The fit parameters for $\gamma(h)$ in (b) are $a = 0.36$, $b = 0.85$, $c = 179$ nm, $d = -0.62 \times 10^{-4}$ nm^{-1}.

These observations are theoretically explained in section 4.3.

4.3. Relation between conventional and differential hardness

We write the following mathematical equivalences:

$$H = F/A_C = (1/A_C)\int \mathrm{d}F = (1/A_C)\int (\mathrm{d}F/\mathrm{d}A_C)(\mathrm{d}A_C/\mathrm{d}h)\,\mathrm{d}h \tag{9}$$

$$HA_C = \int (\mathrm{d}F/\mathrm{d}A_C)(\mathrm{d}A_C/\mathrm{d}h)\,\mathrm{d}h = \int H_d(\mathrm{d}A_C/\mathrm{d}h)\,\mathrm{d}h. \tag{10}$$

Differentiating (10) gives

$$(\mathrm{d}H/\mathrm{d}h)A_C + H(\mathrm{d}A_C/\mathrm{d}h) = H_d(\mathrm{d}A_C/\mathrm{d}h), \tag{11}$$

and after dividing by $(\mathrm{d}A_C/\mathrm{d}h)$

$$H_d = H + (\mathrm{d}H/\mathrm{d}h)A_C/(\mathrm{d}A_C/\mathrm{d}h). \tag{12}$$

Equation (12) is the fundamental relation between H_d and H. It shows that $H_d = H$ for $(\mathrm{d}H/\mathrm{d}h) = 0$, i.e. in case of constant hardness (statement (v) at the end of the last section), and

in the case of a maximum or minimum of H (statement (iii)). Furthermore, we have $H_d > H$ as long as H increases with h (statement (i)), and $H_d < H$ for $\mathrm{d}H/\mathrm{d}h < 0$ (statement (iv)).

Let us now consider the situation of the pure elastic contact (spherical cap). According to Hertz [29, 30] the reduced elastic modulus can be expressed by

$$E_r = 3F/4r_C\delta = 3F/4r_C h. \tag{13}$$

E_r: reduced elastic indentation modulus, r_C: contact radius ($r_C = \sqrt{A_C/\pi}$), δ: elastic deformation depth, $\delta = h = 2h_C$. Furthermore, we can write

$$r_C^2 = h_C(2R_{tip} - h_C) \approx R_{tip}h \qquad \text{for } h << R_{tip} \tag{14}$$

$$r_C = \sqrt{(R_{tip}h)} \tag{15}$$

$$F = (4/3)E_r R^{1/2}h^{3/2} \qquad \mathrm{d}F = 2E_r\sqrt{(R_{tip}h)}\,\mathrm{d}h \tag{16}$$

$$A_C = \pi r_C^2 = \pi R_{tip}h \qquad \mathrm{d}A_C = \pi R_{tip}\,\mathrm{d}h \tag{17}$$

$$H = F/A_C = (4/3\pi)E_r\sqrt{(h/R_{tip})} \sim \sqrt{h} \tag{18}$$

$$H_d = \mathrm{d}F/\mathrm{d}A_C = (2/\pi)E_r\sqrt{(h/R_{tip})} = 1.5H. \tag{19}$$

Equation (19) demonstrates that in the case of a Hertzian elastic contact, H_d develops in the same way as H, and is by a factor of 1.5 larger than H.

Now, it remains to calculate the position h, where the differential hardness H_d achieves its maximum. We differentiate equation (12):

$$\mathrm{d}H_d/\mathrm{d}h = [\mathrm{d}^2H/\mathrm{d}h^2][A_C/(\mathrm{d}A_C/\mathrm{d}h)] + \mathrm{d}H/\mathrm{d}h[2 - A_C(\mathrm{d}^2A_C/\mathrm{d}h^2)/(\mathrm{d}A_C/\mathrm{d}h)^2]. \tag{20}$$

The maximum is obtained for $\mathrm{d}H_d/\mathrm{d}h = 0$. Equation (20) is considerably simplified, if ideal geometries are considered. In the case of a sphere, which will be the case for application of small loads (the indenter is in contact with its spherical cap only), we have (compare equation (17))

$$\mathrm{d}A_C/\mathrm{d}h = \pi R_{tip}, \qquad \mathrm{d}^2A_C/\mathrm{d}h^2 = 0, \qquad [A_C/(\mathrm{d}A_C/\mathrm{d}h)] = h \tag{21}$$

$$\mathrm{d}H_d/\mathrm{d}h = 2(\mathrm{d}H/\mathrm{d}h) + h(\mathrm{d}^2H/\mathrm{d}h^2) = 0 \tag{22}$$

$$2(\mathrm{d}H/\mathrm{d}h) = -h(\mathrm{d}^2H/\mathrm{d}h^2). \tag{23}$$

In figure 8 the curves of $2\mathrm{d}H/\mathrm{d}h$ and $-h(\mathrm{d}^2H/\mathrm{d}h^2)$ are plotted versus h to determine the intersection. Unfortunately, both curves are almost parallel between the two vertical lines inserted into the figure. Hence the intersection point is difficult to determine—it lies somewhere between the vertical lines, i.e. $h(H_{d,max}) = (24 \pm 3)$ nm. This result is in good agreement with the maximum position of H_d in figures 7(c) and (d) around 25 nm.

At the end of this section we want to simplify the fundamental relation between H_d and H (equation (12)) for spheres and ideal pyramids/cones, respectively.

According to equations (17) and (21) we have $[A_C/(\mathrm{d}A_C/\mathrm{d}h)] = h$, consequently

$$H_d = H + h(\mathrm{d}H/h) \qquad \text{for spherical indents.} \tag{24}$$

For a cone/pyramid, there is $A_C = C_A h_C^2$, and

$$\mathrm{d}A_C/\mathrm{d}h = (\mathrm{d}A_C/\mathrm{d}h_C)(\mathrm{d}h_C/\mathrm{d}h) = 2C_A h_C(\mathrm{d}h_C/\mathrm{d}h) \approx 2C_A h_C^2/h = 2A_C/h \tag{25}$$

$$[A_C/(\mathrm{d}A_C/\mathrm{d}h)] = h/2 \tag{26}$$

$$H_d = H + (h/2)(\mathrm{d}H/\mathrm{d}h) \qquad \text{for pyramids and cones.} \tag{27}$$

Equation (24) means that for a spherical indent H is the linear average of H_d:

$$H = (1/h)\int H_d\,\mathrm{d}h \qquad \text{for spherical indents.} \tag{28}$$

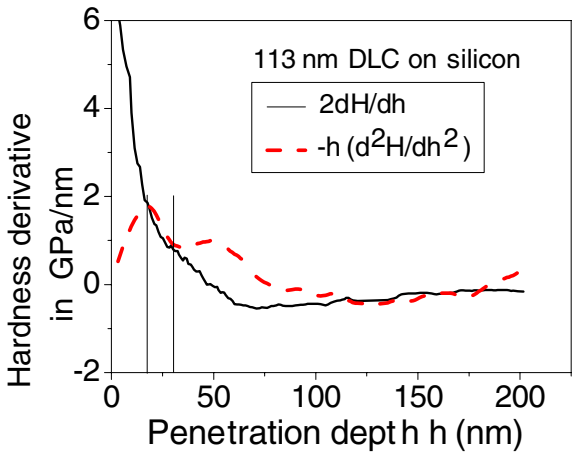

Figure 8. Graphical solution of the equation $2(\mathrm{d}H/\mathrm{d}h) + h(d^2H/\mathrm{d}h^2) = 0$. The resulting depth h is situated somewhere between the two inserted vertical lines since the intersection of the drawn curves is badly defined.

It follows that $hH = \int H_d \,\mathrm{d}h$, and after differentiation $H + h(\mathrm{d}H/\mathrm{d}h) = H_d$ in accordance with equation (24).

Equations (24) and (27) show that $H_d - H \sim h(\mathrm{d}H/\mathrm{d}h)$. The coincidence of H and H_d at deep penetrations requires that $\mathrm{d}H/\mathrm{d}h$ diminishes with increasing h more rapidly than $1/h$. Otherwise the difference $H_d - H$ would increase with deeper indentations. The model of geometrically necessary dislocations predicts that $H \sim h^{-1/2}$, resulting in $\mathrm{d}H/\mathrm{d}h \sim h^{-3/2}$. This model guarantees that the difference between H_d and H vanishes for large depths. One notes, however, that the vanishing of the difference between conventional and differential hardness is a slow process, and the depths, attainable by our nanoindentation equipment, are too small to achieve equivalent values of H and H_d.

To summarize, a depth-dependent contact pressure, i.e. a situation $(\mathrm{d}H/\mathrm{d}h) \neq 0$, is the deeper reason for differences between H and H_d. Equation (12) shows that $H_d > H$ for $(\mathrm{d}H/\mathrm{d}h) > 0$. Apart from situations 'soft layer on hard substrate', this applies to the initial state of every indentation where the contact is purely elastic. As long as the indenter tip is far from the substrate, the contact pressure is zero. Consequently, the contact pressure must always start at zero, and it increases with increasing penetration depth. After yielding, the hardness can further increase owing to the transition from spherical to pyramidal contact. This transition results in a reduction of the effective full apex angle ψ. According to the models of Johnson [31] and Tanaka [32], the hardness increases with $\cot(\psi/2)$, i.e. a sharper indentation results in a higher effective strain, which in turn gives rise to a higher hardness. The described scenario explains the hardness evolution of Berkovich indents into the thick DLC layer on silicon, depicted in figure 6, as well as the first states of indentation of figure 7.

In situations, characterized by $(\mathrm{d}H/\mathrm{d}h) < 0$, we find $H_d < H$. This is typical for the ISE in homogeneous materials, as for copper (figure 2). Furthermore, it applies to sufficiently deep indents into hard layers on soft substrates, as the late indentation states of figure 7.

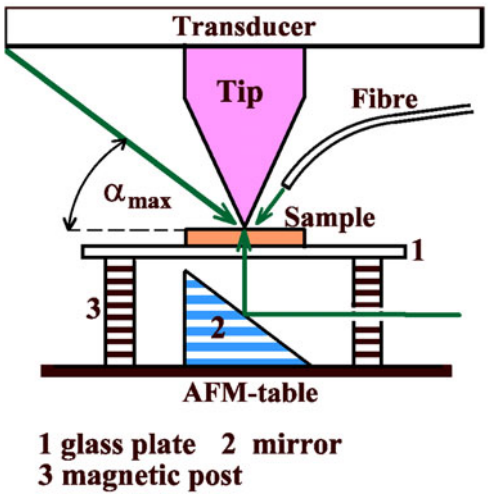

Figure 9. Experimental set-up for photoplastic experiments. The transparent sample is glued to a glass plate (1). It is illuminated by laser light reflected at the mirror (2). Alternatively the sample can be illuminated using a fibre guide, or by direct illumination. In the latter case the transducer geometry limits the angle of incidence to $\alpha_{max} \approx 20^\circ$. Furthermore, illumination from the top results in unwanted shadowing by the diamond tip.

5. Advantageous applications of differential hardness

Let us first emphasize that hardness, and depth sensing nanohardness in particular, is not a material property. It is an experimental parameter, namely the mean contact pressure beneath the indenter, from which 'true' physical properties must be extracted. Equations (18) and (19) show how for the elastic contact the 'true' physical property elastic modulus can be inferred from H and H_d, respectively. For very large indents, where H and H_d are constant, the yield stress can be extracted from hardness (equation (6)), provided that the constraint factor is known. Extraction of physical units from hardness is particularly difficult in the transition area from elastic to plastic deformation. The differential hardness is a good indicator of the beginning of yielding in the absence of discontinuities (pop-ins). Since after onset of yielding the material is more easily deformed, H_d as a measure of current properties reacts first. H_d does not increase any further, and may even decrease after yielding, whereas H may further increase. This is particularly obvious in figures 7(c) and (d), where yielding starts at a depth of about 25 nm. At this depth H_d has a distinct maximum, whereas H continues to slowly increase.

Since H_d is a measure of the momentary deformation resistance, it proves particularly useful for situations where external factors, influencing the hardness, are changed during the indentation process. Such a factor is the sample temperature. However, depth-sensing hardness measurements under conditions of simultaneous temperature change are difficult to perform, mainly due to thermal drift. It is therefore better to look for athermal factors that can modify the hardness during the indentation process. An interesting possibility of reversible hardness modification is the application of light. In semiconductors of sphalerite structure (ZnS structure) small intensities (some mW cm^{-2}) of light of appropriate wavelengths can induce the so-called photoplastic effect [20]–[22], [33, 34]. In this class of materials, dislocations can be electrically

charged (this is a consequence of the fact that the (111) sliding planes are polar planes, i.e. consist of one kind of atom only). Mobile charge carriers, generated by the internal photoelectric effect, can move to dislocations and may alter the dislocation charge. As a consequence, electrostatic forces between dislocations, between dislocations and electrically active point defects, or between dislocations and the entire crystal lattice are changed. This results in a change of the dislocation mobility, and consequently in a variation of the hardness. The hardness can increase under illumination (positive photoplastic effect), as is very often found with II–VI-semiconductors, or it can decrease during illumination (negative photoplastic effect), as often found with III–V-semiconductors [35]. We investigated the positive photoplastic effect of the II–VI-semiconductor ZnSe owing to laser illumination at a wavelength $\lambda = 524$ nm. The sample, mounted on a transparent sample holder, was illuminated from below as illustrated in figure 9. The light was focused to a small spot directly beneath the indenter tip. The heat generated in the light spot distributes over the sample surface. Thus the total heat energy, absorbed by the sample, can be kept very small, even for high light intensities. The total temperature increase was found to be less than 10^{-2} K. In figure 10 details of two load–depth curves into ZnSe, using a Berkovich indenter, are shown. The total load for both curves is 16 mN. Curve 2 represents an indent in permanent darkness whereas curve 1 displays the situation where the indent started in darkness, and where at a total depth of 600 nm the laser light was turned on. The light resulted in a prompt dramatic increase of the slope of the load–depth curve $F(h)$. The total depth for a load $F = 16$ mN in permanent darkness is $h_2 = 664$ nm, whereas the illumination reduced the depth to $h_1 = 637$ nm. At these large depths, the pyramid is almost ideal, i.e. $A_C \sim h^2$, $H \sim F/h^2$. A depth decrease by Δh results in a relative hardness increase

$$\Delta H/H = -2\Delta h/h. \tag{29}$$

We find $\Delta H/H \approx 8\%$ in our experiment. This is not very much since the illumination was started close to the end of the indentation process. When comparing indents that were conducted under permanent darkness and under permanent illumination, respectively, the difference is $\Delta H/H \approx 21\%$. In contrast to this, the change of the differential hardness is much stronger when turning the light on. In figure 10 the slope of the loading curve at $h = 600$ nm is $(\mathrm{d}F/\mathrm{d}h)_{[2]} = 3.7 \times 10^4$ N m^{-1} for curve 2 (permanent darkness) and $(\mathrm{d}F/\mathrm{d}h)_{[1]} = 7.4 \times 10^4$ N m^{-1} for curve 1 (laser light turned on), i.e. there is a slope increase by a factor of two. From equation (8) one concludes that there is an increase of the differential hardness by a factor of 2, too.

6. Summary

The key to separation of elastic and plastic contributions to the indenter penetration is the knowledge of the relation between contact depth h_C and total depth h_t. Unfortunately, the ratio h_C/h_t is not a constant, but changes with depth, since at the initial state of indentation the contact is purely elastic, and with increasing load the plastic part increases. Multicycling testing delivers a set of data pairs (h_C, h_t), from which a continuous function $h_C(h)$ can be constructed by data fitting. This allows us to calculate the conventional hardness $H(h) = F(h)/A_C(h)$ as a continuous function of depth from a single indent. Instead of H a differential hardness $H_d = \mathrm{d}F/\mathrm{d}A_C$ can be considered, which is a measure of the current deformation resistance. The difference $H_d - H$ was found to be proportional to $(\mathrm{d}H/\mathrm{d}h)$. An overall equivalence of H_d and H requires a constant hardness. In all other cases H_d equals H at the extrema of H only. For situations with $\mathrm{d}H/\mathrm{d}h > 0$ a relation $H_d > H$ was found, whereas the normal ISE $(\mathrm{d}H/\mathrm{d}h < 0)$ results in a differential hardness smaller than the conventional hardness.

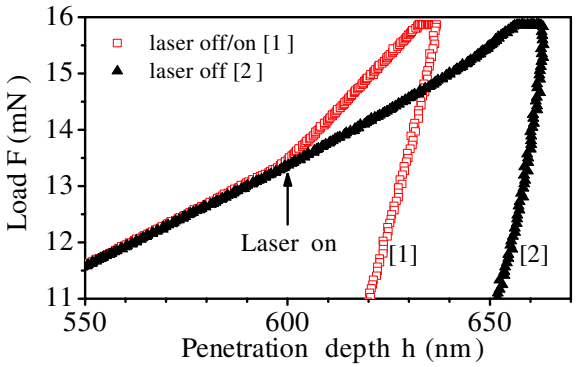

Figure 10. Response of the load–depth curve of a Berkovich nanoindent into ZnSe(111) to sudden illumination by laser light (λ = nm, intensity I = 120 mW cm^{-2}). Curve 1: starting the indent in darkness the laser was turned on at a total depth $h = 600$ nm. Curve 2: indentation in permanent darkness.

Acknowledgments

This work was performed within the frame of the project 'Quality assessment of thin layers and composite material', supported by the Federal Country Brandenburg. The authors gratefully acknowledge technical support by R Ries and K Kubica, crystallographer and metallography expert, respectively, in the Wildau Surface Technology Labs. DLC-coated samples were provided by Dr Weihnacht, Fraunhofer Institute IWS Dresden. Further support by Professor Paufler, TU Dresden, IKFP, and by Professor Vehoff and Dr Goeken, Universität des Saarlandes, Saarbrücken, is highly appreciated. Financial aid by 'Deutsche Akademie der Naturforscher Leopoldina' Halle (Saale) is also gratefully acknowledged.

References

[1] Tabor D 1951 *The Hardness of Metals* (Oxford: Clarendon)
[2] Mott B W 1956 *Microindentation Hardness Testing* (London: Butterworth)
[3] Hay J L and Pharr G M 2000 Instrumented indentation testing *ASM Metals Handbook* (Materials Park, OH: ASM International)
[4] Burnham N A and Colton R J 1989 J *Vac. Sci. Technol.* A **7** 2906
[5] Hues S M, Draper C F, Lee K P and Colton R J 1994 *Rev. Sci. Instrum.* **65** 1561
[6] Hues S M, Draper C F and Colton R J 1994 *J. Vac. Sci. Technol.* B **12** 2211
[7] Nanoindenter XP by MTS Systems Corporation, 14000 Technology Drive, Eden Prairie, MN 55344-2290, USA, http://www.mts.com/
[8] Triboindenter and Triboscope by Hysitron Inc., 5251 West-73rd Street, Minneapolis, MN 55439, USA, http://www.hysitron.com/
[9] Oliver W C and Pharr G M 1992 *J. Mater. Res.* **7** 1564
[10] Doerner M F and Nix W D 1986 *J. Mater. Res.* **1** 601
[11] Domnich V and Gogotsi Y 2002 *Rev. Adv. Mater. Sci.* **3** 1
[12] Wolf B, Richter A and Günther M 2003 *Z. Metallkd.* **94** (7)
[13] Wolf B, Bambauer K-O and Paufler P 2001 *Mater. Sci. Eng.* A **298** 284
[14] Bahr D F, Wilson D E and Crowson D A 1999 *J. Mater. Res.* **14** 2269
[15] Mann A B and Pethica J B 1999 *Phil. Mag.* A **79** 577
[16] Michalske T A and Houston J E 1998 *Acta Mater.* **46** 391

[17] Elmustafa A A, Eastman J A, Rittner M N, Weertman J R and Stone D S 2000 *Scr. Mater.* **43** 95
[18] Elmustafa A A and Stone D S 2002 *Acta Mater.* **50** 3641
[19] Elmustafa A A and Stone D S 2003 *J. Mech. Phys. Solids* **51** 357
[20] Wolf B, Belger A, Meyer D C and Paufler P 2001 *Phys. Status Solidi* a **187** 415
[21] Wolf B, Meyer D C, Belger A and Paufler P 2002 *Phil. Mag.* A **82** 1865
[22] Osip`yan Yu, Petrenko V F, Zaretskij A V and Witworth R W 1986 *Adv. Phys.* **35** 115
[23] Bhushan B, Kulkarni A V, Bonin W and Wyrobek J T 1996 *Phil. Mag.* A **74** 1117
[24] CrysTec GmbH Kristalltechnologie, Köpenicker Straße 325, 12555 Berlin
[25] Nix W D 1997 *Mater. Sci. Eng.* A **234–236** 37
[26] Nix W D and Gao H 1998 *J. Mech. Phys. Solids* **46** 411
[27] Richter A, Ries R, Smith R, Henkel M and Wolf B 2000 *Diam. Relat. Mater.* **9** 170
[28] Gilman J J 1971 *The Science of Hardness Testing and its Research Applications* ed J H Westbrook and H Conrad (Metals Park, OH: American Society for Metals) pp 54–8
[29] Hertz H 1882 *J. Rein. Angew. Math.* **92** 156
[30] Johnson K L 1985 *Contact Mechanics* (Cambridge: Cambridge University Press)
[31] Johnson K L 1970 *J. Mech. Phys. Solids* **18** 115
[32] Tanaka K 1987 *J. Mater. Sci.* **22** 1501
[33] Koubaiti S, Couderc J J, Levade C and Vanderschaeve G 2000 *Phil. Mag.* **80** 83
[34] Koubaiti S, Couderc J J, Levade C and Vanderschaeve G 1996 *Scr. Mater.* **34** 869
[35] Takeuchi S, Maeda K and Nagakawa K 1983 Defects in semiconductors II *MRS Symp. Proc.* vol 14, ed S Mahajan and J W Corbett (New York: North-Holland)